Journal of
Materials Chemistry C

PAPER

View Article Online
View Journal | View Issue

Published on 04 March 2014. Downloaded by Western Kentucky University on 29/10/2014 15:19:48.

Cite this: *J. Mater. Chem. C*, 2014, **2**, 3928

Substituent effect on the crystal packing and electronic coupling of tetrabenzocoronenes: a structure–property correlation†

Chi-Hsien Kuo,[a] Ding-Chi Huang,[b] Wei-Tao Peng,[a] Kenta Goto,[c] Ito Chao*[a] and Yu-Tai Tao*[ab]

Received 13th February 2014
Accepted 4th March 2014

DOI: 10.1039/c4tc00296b

www.rsc.org/MaterialsC

Tetrabenzo[*a*,*d*,*j*,*m*]coronene (TBC) is a contorted polyaromatic molecule which shows near co-facial $\pi-\pi$ stacking in the crystalline state and the high electronic coupling resulting from the packing renders it a potential candidate as a transistor material. Substitution at the periphery perturbs the packing due to steric as well as dipolar interactions and thus changes the electronic coupling between neighbouring molecules. In the light of the high sensitivity of charge mobility toward electronic coupling, a new series of TBC derivatives with substituents at 1-, 2-, 3-, 6-, 7-, 8-positions were designed, synthesized, and characterized. Needle-like single crystals were prepared using the physical vapor transport (PVT) method for these unsymmetrically substituted derivatives and were used for crystal structure analyses as well as the single crystal field-effect transistor (SCFET) device fabrication. The derivatives with fluoro-containing substituents exhibit anti-parallel cofacial or slightly shifted $\pi-\pi$ stacking, whereas those with bulky alkyl substituents show skewed and more significantly shifted $\pi-\pi$ stacking. A systematic comparison of the crystal packings and the calculated electronic couplings/charge mobilities with the measured SCFET mobilities shows a rough correlation and sheds light on the origin of the large hole-mobility of the SCFET with hexa-fluorinated TBC as the channel material.

Introduction

Organic field-effect transistors (OFETs) have attracted much attention due to their potential applications in cost effective flexible organic electronics.[1] The versatility in structural manipulation also makes OFETs a common approach for studying the field-dependence charge transport behaviors. Considerable effort has been devoted to enhancing the charge carrier mobility (μ) through the design of a novel class of organic semiconductor materials[2] as well as the exploration of new OFET structures *via* selection or modification of dielectric materials and electrodes.[3] However, a fundamental understanding of the physical parameters affecting the mobility, particularly the correlation between molecular structure/crystal packing and charge carrier mobility, is still limited mainly owing to the complexity of the morphology involved in a thin film deposited at the substrate surface. On the other hand, organic single-crystal field-effect transistors (SCFETs)[4] offer the opportunity to explore the intrinsic charge transport properties in organic semiconductors, since the aforementioned extrinsic effects associated with polycrystalline films can be minimized in single crystal devices. A comparison of properties obtained with single crystal devices would enable a systematic study on the structure–property correlation, delineating the effect of dielectric surfaces on charge transport.[5] Among the p-type SCFETs reported, rubrene yields the highest reproducible hole mobility of up to 20 cm^2 V^{-1} s^{-1}, and a dependence of mobility on the choice of gate dielectric and the direction of measurement were clearly demonstrated.[6] To date, the compounds which have the highest electron mobility reported are SCFETs of *N*,*N*′-bis(*n*-alkyl)-(1,7 and 1,6)-dicyanoperylene-3,4:9,10-bis(dicarboximide) (PDIF-CN2) and 5,7,12,14-tetrachloro-6,13-diazapentacene (TCDAP), both with mobilities of a few cm^2 V^{-1} s^{-1}.[7]

The charge transport between neighboring organic molecules has been suggested to be determined by the transfer integral (or electronic coupling) between the molecules, as well as the reorganization energy involved in neutral/charged state transformation for that particular molecule.[8] It is widely accepted that a minimization of reorganization energy and a maximization of the transfer integral is preferred in molecular design. However, it is also demonstrated by theoretical calculation that the transfer integral is highly sensitive to the relative disposition of the neighboring molecules due to overlap of the nodal regions of the highest occupied molecular orbitals

---

[a] *Institute of Chemistry, Academia Sinica, Taipei, Taiwan, Republic of China*
[b] *Department of Chemistry, National Tsing-Hua University, Hsin-chu, Taiwan, Republic of China*
[c] *Institute of Materials Chemistry and Engineering (IMCE), Kyushu University, Fukuoka, 812-8581, Japan*

† Electronic supplementary information (ESI) available: Details of synthetic details and theoretical calculation are available. See DOI: 10.1039/c4tc00296b

This journal is © The Royal Society of Chemistry 2014

Published on 04 March 2014. Downloaded by Western Kentucky University on 29/10/2014 15:19:48.

(HOMOs) or the lowest unoccupied molecular orbitals (LUMOs), so that the highest transfer integral occurs for perfect face-to-face packing[9] and diminishes or vanishes for shifted π-stacking. Yet the co-facial π-stacking is usually not favored due to quadrupole repulsion for aromatic compounds.[10] This is evidenced by the common herringbone packing motif for most unsubstituted linear acenes and oligothiophenes. Substitution with polar groups or bulky groups at the periphery of the linear aromatics perturbs the packing for dipolar interactions or steric interactions in a subtle way that the prediction of the packing of organic molecules is challenging. The packing in turn affects the morphology of the crystal that is grown.[11]

Contorted polyaromatics are conceived to have a high tendency to pack face-to-face due to the potential of self-complementary packing.[12] A number of non-planar polycyclic aromatic hydrocarbons have been shown to exhibit cofacial stacking in single crystals.[13] 1,2,3,4,7,8,9,10-Tetrabenzocoronene (TBC) is one such class of non-planar (or contorted) molecules due to the proximity of several C–H bonds.[14] 2,7,12,17-Tetraoctyl substituted TBC showed strong long-range ordered π-stacking in the solution state by forming nanofibers, implying a co-facial packing. We have also demonstrated recently that the TBC derivatives which bear four fluoro groups (**TFTBC**) or four chloro groups (**TCTBC**) at the symmetrical 2,7,12,17-positions exhibit near cofacial π–π stacking, while the one with four methyl substituents exhibits significantly shifted π–π stacking. Transistors based on their single crystal exhibit a high field-effect mobility from 0.1 to 0.7 $\mathrm{cm^2\,V^{-1}\,s^{-1}}$ with a good structure–property correlation in comparison to the theoretical calculations.[15] With the four substituents distributed at the opposite sides of the molecule, an inevitable steric interaction determines the relative shifts in the otherwise co-facial packing of neighboring molecules. It is contemplated that with unsymmetrical substitutions, which generate a molecular dipole moment, a new attractive molecular interaction and relaxation of steric repulsion may result in a structural motif that enhances electronic coupling and thus charge transport.

We report herein the synthesis and structure characterization of a new series of TBC derivatives, with substituents at 1-, 2-, 3-, 6-, 7-, 8-positions (**1a–h**, Fig. 1) so that the molecules are unsymmetrical. Single crystal structures were determined for all eight derivatives. Needle-like crystals along the π–π stacking direction were obtained. Cofacial or shifted π–π stacking was observed from crystal structure analysis. Theoretical calculations on the hole mobility along the π–π stacking direction were carried out and experimental investigations were performed based on the SCFET configuration for a systematic comparison of charge transport properties among various substituted derivatives. The field-effect mobility was measured and a correlation with the theoretical results is discussed.

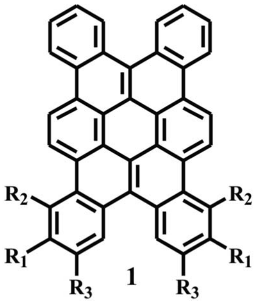

$R_1 = R_2 = R_3 = H$, **1a**
$R_1 = F$, $R_2 = R_3 = H$, **1b**
$R_1 = Cl$, $R_2 = R_3 = H$, **1c**
$R_1 = CH_3$, $R_2 = R_3 = H$, **1d**
$R_1 = CF_3$, $R_2 = R_3 = H$, **1e**
$R_1 = C(CH_3)_3$, $R_2 = R_3 = H$, **1f**
$R_1 = H$, $R_2 = R_3 = F$, **1g**
$R_1 = R_2 = R_3 = F$, **1h**

Fig. 1 Molecular structure of substituted tetrabenzo[*a*,*d*,*j*,*m*]coronene (**1**).

Experimental and computational details

The series of derivatives of **1** were synthesized in the laboratory (the synthetic details are provided in the ESI†). Except for alkylated compounds **1d** and **1f**, which were additionally characterized by NMR, the rest were characterized by mass, elemental analyses and X-ray crystallography owing to their poor solubility in common organic solvents. Single crystals were grown in a temperature-gradient copper tube by a vapor-phase transfer method with argon as the carrier gas.[16] The X-ray diffraction was carried out mostly on a Bruker X8APEX X-ray diffractometer with Mo Kα radiation ($\lambda = 0.71073$ Å) and the structure was solved by SHELX 97 program. For compounds **1d** and **1f**, the X-ray data were collected on a Rigaku RAPID-HR Imaging Plate diffractometer with graphite monochromated Mo Kα radiation ($\lambda = 0.71069$ Å) and a Rigaku Saturn724 diffractometer using multi-layer mirror monochromated Mo-Kα radiation ($\lambda = 0.71075$ Å). The structure was solved using the direct method technique (SIR 2004 and SHELXL97) and a full-matrix least squares refinement based on F^2.

Devices were fabricated in a similar fashion as described in our previous publication.[15] In brief, the top-contact, top-gate SCFET was prepared by placing the single crystal on a glass substrate, which was modified with a monolayer of *n*-octadecyltrichlorosilane (ODTS). Painted colloidal graphite was used as the source and drain electrodes. A thin film of parylene-N (~2–4 μm thick) was deposited on top of the crystal in a home-made reactor as the insulating dielectric. Finally, colloidal graphite was painted on top of the parylene film as the gate electrode. The channel length and width of devices varied depending on the dimensions of crystals chosen. These parameters, as well as the thickness of parylene, were determined for each individual device by using a Veeco Daktak 150 Stylus profiler. The electrical characteristics of the devices were measured in an ambient atmosphere in a dark chamber using a computer-controlled Agilent 4156C Semiconductor Parameter Analyzer. The field-effect mobility of the OFET devices was calculated from the *I*–*V* characteristics in the saturation region ($I_{\mathrm{SD,sat}}$) according to eqn (1):[17]

$$I_{\mathrm{SD,sat}} = (WC_{\mathrm{i}}/2L)\mu_{\mathrm{sat}}(V_{\mathrm{G}} - V_{\mathrm{th}})^2 \tag{1}$$

where W and L are the channel width and length respectively, and C_{i} is the capacitance per unit area of the parylene-N insulator, V_{G} is the gate voltage and V_{th} is the threshold voltage.

A computational procedure for calculating the charge carrier mobility has been elaborated previously.[18] Briefly, the

Published on 04 March 2014. Downloaded by Western Kentucky University on 29/10/2014 15:19:48.

calculations of internal reorganization energy (λ) of **1a–h** were performed with the Gaussian 09 program[19] at the level of B3LYP/6-31G(d,p).[8,20] The transfer integral (t) between neighboring dimer pairs in the crystal structure was calculated with ADF[21] at the PW91PW91/DZP level of theory.[22] With λ and t, Marcus theory for self-exchange electron transfer was used to obtain the carrier transport rate at 300 K. With the rate and the intermolecular distance obtained from the crystal structure, the carrier diffusion coefficient was deduced and used in the Einstein relationship to derive the carrier mobility. Although the equation has certain limitations such as the neglection of nuclear tunneling effect and the nonlocal couplings, it can be deemed acceptable for the purposes of qualitative analysis and molecular design.[23] It is noted that the X-ray coordinates of **1b** and **1g** are with disorders for the fluorine atoms and the hydrogen atoms at the corresponding positions (*e.g.*, 2,7-positions of **1b** and 1,3,6,8-positions of **1g**). Because of the uncertainty of the F/H positions, while calculating t for these two molecules, the C–F bond length and C–H bond length at corresponding positions were fixed at 1.350 and 0.965 Å, respectively. Parallel and antiparallel dimeric relationships were both considered for **1b** and **1g**, but they do not change the magnitude of t significantly. For **1f** and **1h**, there are nonequivalent dimer relationships along the 1-D charge-transporting-stacking direction. Because a charge can only move along this channel, the smallest t among the dimers will result in a bottleneck of the 1-D charge transport. This t is used in Table 2 to give a rough estimate of the charge mobility. For all the calculation results, see the ESI.†

Results and discussion

Except for the parent compound **1a**, whose synthesis and characterization have been described in our previous publication,[15] the synthetic approach of unsymmetrical compound **1b–h** is summarized in Scheme 1. In brief, Corey–Fuchs[24] reaction was first carried out by treating the commercially available 10-diphenylmethylene-9(10*H*)-anthracenone with triphenylphosphine and carbon tetrabromide to afford compound **2**. Suzuki–Miyaura[25] reaction between **2** and substituted boronic acid led to the key intermediate bisolefin **3b–h**, respectively. Oxidative dehydrogenation of **3** gave a mixture of half-cyclized products which, without isolation, were converted into fully cyclized products **1** by Scholl cyclization using $FeCl_3$ as the catalyst.[26] All products were purified by vacuum-sublimation and obtained in good yield.

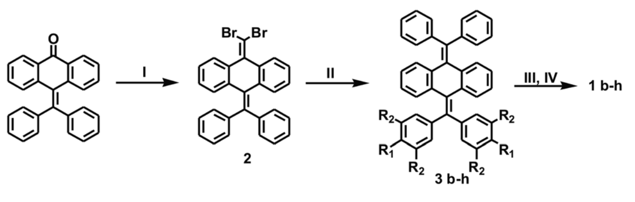

Scheme 1 Synthesis of tetrabenzocoronenes with unsymmetrical substitutions. Reagents and conditions: (I) CBr_4, PPh_3, 80 °C; (II) boronic acid, K_2CO_3, $Pd(PPh_3)_4$, toluene, ethanol/H_2O; (III) I_2, propylene oxide, benzene, *hν*; (IV) $FeCl_3$, CH_2Cl_2.

Characterization

The compounds appear yellow (**1a–d**, **1f**) to orange yellow (**1e**, **1g**, and **1h**). Except for compounds **1g** and **1h**, which were not soluble in any common organic solvents, similar UV-Vis absorption spectra of compound **1a–f** in dichloromethane exhibiting multiple λ_{max} were obtained in the 300–500 nm region (Fig. 2). The p-band ($\pi \rightarrow \pi^*$ transition) in the long wavelength region for compound **1a** occurs at 423 nm. A small substituent effect on the absorption maximum can be observed, with di-chloro (**1c**), di-methyl (**1d**), di-trifluoromethyl (**1e**), and di-*t*-butyl (**1f**) substitution giving a red-shift (~3–4 nm) and di-fluoro (**1b**) substitution giving blue-shift (~3 nm) relative to that of the parent compound. Very weak α-band ($n \rightarrow \pi^*$) was discernible for all six compounds at ~456–458 nm.

The HOMO energy levels for compound **1** were measured using a photoelectron spectrometer (AC2) in the solid state. The HOMO levels ranged from 5.17 to 6.09 eV, with electronegative substituents such as fluorine and chlorine shifting the HOMO level down and a donation group such as methyl and a *t*-butyl group shift the HOMO level up. This is in good accordance with the inductive effect of substituents. The results are summarized in Table 1.

Thermal gravimetric analyses showed that the series of compounds have excellent thermal stability with decomposition temperature (5 to 8% weight loss) at around 470 °C and above in a nitrogen atmosphere, as illustrated in Fig. 3.

Crystal structure analyses and theoretical results

All eight compounds give needle-like crystals. X-ray analyses revealed a contorted geometry as expected. Similar to our previous observations, the contorted molecules have two stereoisomers.[15] One has two benzenoids in the right side pointing in the same direction and opposite to the two in the left side, as illustrated in Fig. 4a. Compounds **1a–c**, **1g**, and **1h**,

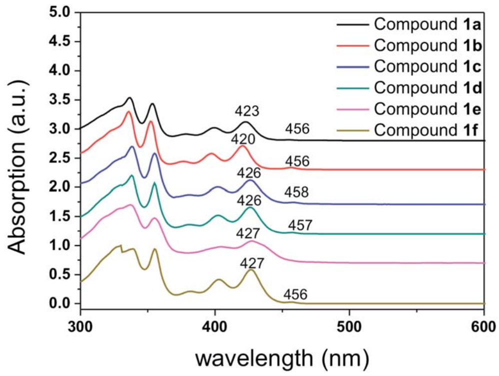

Fig. 2 UV-Vis spectra for **1a–f**.

Table 1 HOMO energy levels of tetrabenzocoronenes derivatives

	1a	1b	1c	1d	1e	1f	1g	1h
HOMO (±0.1 eV)	5.4	5.6	5.5	5.5	6.1	5.2	5.6	5.8

This journal is © The Royal Society of Chemistry 2014

Published on 04 March 2014. Downloaded by Western Kentucky University on 29/10/2014 15:19:48.

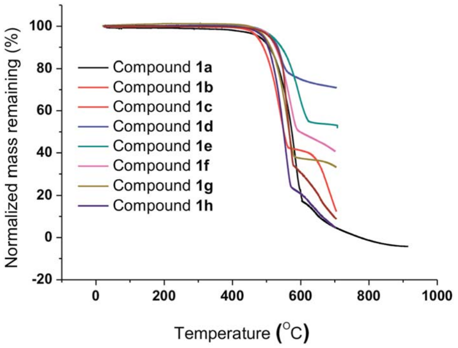

Fig. 3 Thermal gravimetric analyses of **1**.

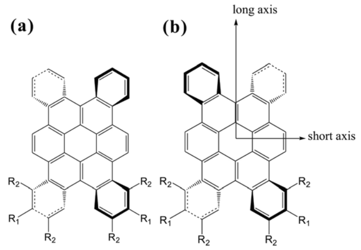

Fig. 4 (a) The structure observed for TBC with small substituents (**1a–c**, **1g**, and **1h**). (b) The structure observed for TBC with bulky substituents (**1d–f**).

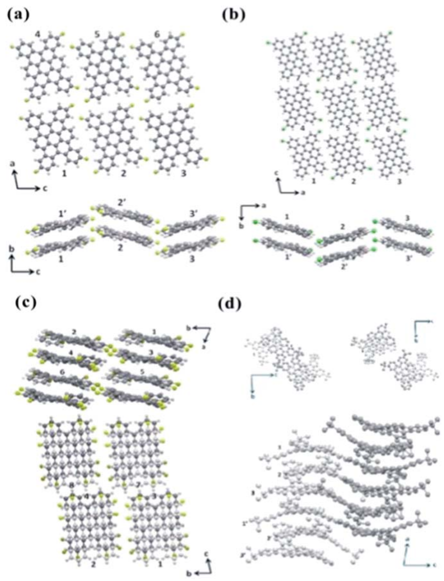

Fig. 5 (a) Crystal packing of **1b** viewed from the top of the molecules (*b* axis) and down the long molecular axis (*a* axis), respectively. Because of disorders in the X-ray coordinates, half-occupancies of hydrogen and fluorine atoms are found at the 2,7,12,17-positions. (b) Crystal packing of **1c** viewed from the top of the molecules (*b* axis) and down the long molecular axis (*c* axis), respectively. (c) Crystal packing of **1h** viewed down the long molecular axis (*c* axis) and from the top of the molecules (*a* axis), respectively and (d) crystal packing of **1f** viewed from the top of the molecules (*a* axis) and down the *b* axis, respectively.

which bear compact substituents (H, F, and Cl) adopt this geometry. In contrast, compounds **1d–f**, which bear bulky substituents (CH_3, CF_3, *t*-butyl, respectively), have the two benzenoids in each side pointing in the opposite direction (Fig. 4b).

Among the compounds with small substituents, **1a**, **1b**, **1c**, and **1g** pack nearly face-to-face with π–π stacking distances of 3.64–3.66 Å and centroid-to-centroid distances of 3.75–3.77 Å (Fig. 5a and b and Table 2). The spatial arrangement of crystal packing for minimizing the steric repulsion and maximizing intermolecular interactions leads to a shift of molecular packing between layers, which can be described with displacements along the long (d_l) and short (d_s) molecular axes. For the parent compound **1a**, dihalogenated **1b**, **1c**, and tetrafluorinated **1g**, the d_l values are between 0.01 and 0.19 Å, and the d_s values are between 0.86 and 0.96 Å. This pattern of π-stacking with a more significant shift along the short axis than the long axis is similar to that of 2,7,12,17-tetrafluoro- and tetrachloro-TBCs we reported previously (**TFTBC** and **TCTBC** in Table 2).[15] Compared to the perfectly face-to-face sandwich packing, shifting along the short molecular axis can effectively alleviate the H⋯H repulsions between the upward/downward pointing hydrogen atoms at the 4,5,14,15-postions of two contorted TBC molecules. Take the parent compound (**1a**) as an example, if two **1a** molecules were held in the sandwich packing position with the π–π distance found in crystal (3.66 Å), close H⋯H contacts would be found (2.02 Å, as shown in Fig. 6). Whereas in the crystal structure the distance between the same pair of hydrogen atoms is 2.642 Å, which is larger than the sum of the van der Waals radii (2.4 Å). In contrast, compound hexafluorinated **1h** exhibits shifted π–π stacking mainly along the long molecular axis with its d_l value as large as 1.96 Å and a rather small d_s value (0.24 Å; Fig. 5c; Table 2). Shifting along the long molecular axis also can avoid the H⋯H repulsions just mentioned. The possibility of an additional electrostatic driving force for shifting along the long axis is implied by the molecular electrostatic potential (MEP) of **1h**, which features an electropositive face and an electronegative edge due to extensive fluorination (Fig. 7a). By shifting along the long axis, the electropositive face can interact with the electronegative face of the antiparallel molecule in the next layer, and the electronegative fluorine edge along the long molecular axis can interact with the electropositive hydrogen edge in the next layer (Fig. 7b).

It is noted that compounds **1b** and **1g** have disorders in their crystal structures, probably due to packing in an anti-parallel manner between layers (Fig. 5a). This anti-parallel packing appears in another fluoro-substituted compound **1h**, but without crystal disorder. The dichloro-substituted **1c**, however, packs parallel between layers probably due to Cl⋯Cl and Cl⋯H interactions (Fig. 5b). Comparing the crystal structures of unsymmetrical **1b**, **1c** and **1g** to those of symmetrical substituted 2,7,12,17-tetrachloro-TBC (**TCTBC**) and 2,7,12,17-tetrafluoro-TBC (**TFTBC**),[15] one would notice that the dipole–dipole interaction is not a determining factor for crystal engineering of TBCs toward close π-stacking for stronger coupling. First of all, unsymmetrical **1g** packs in an anti-parallel manner as one would expect by considering an ideal arrangement of

Published on 04 March 2014. Downloaded by Western Kentucky University on 29/10/2014 15:19:48.

Table 2 Intermolecular distances along the cell axis relevant to π-stacking (d_{axis}), π–π stacking distances measured with the use of molecular mean planes ($d_{\pi-\pi}$), molecular centroid-to-centroid distances ($d_{\text{c-c}}$), short molecular axis shifts (d_{s}), long molecular axis shifts (d_{l}) in the crystal structures and the calculated reorganization energies (λ^+), electronic couplings (t^+), and mobilities (μ^+) for hole transport

Compounds	d_{axis} (Å)	$d_{\pi-\pi}$ (Å)	$d_{\text{c-c}}$ (Å)	d_{s} (Å)	d_{l} (Å)	λ^+ (meV)	t^+ (meV)	μ^+ (cm^2 V^{-1} s^{-1})
1a	3.77	3.66	3.77	0.87	0.01	132	41	0.58
1b	3.77	3.66	3.77	0.87	0.19	151	22	0.13
1c	3.77	3.64	3.77	0.96	0.17	143	22	0.15
1d	3.74	—	4.23	—	—	134	7	0.02
1e	3.65	—	4.00	—	—	148	35	0.33
1f	3.84	—	6.39	—	—	136	40	0.56
1g	3.75	3.65	3.75	0.86	0.01	135	41	0.56
1h	3.58	3.58	4.06	0.24	1.96	147	59	0.91
TFTBC	3.72	3.61	3.72	0.84	0.34	169	41	0.36
TCTBC	3.75	3.63	3.75	0.76	0.55	154	51	0.68
TMTBC	3.66	—	4.39	—	—	136	20	0.13

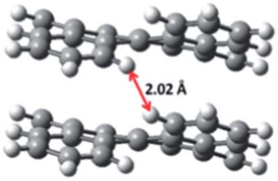

Fig. 6 Close H⋯H contacts found in a pair of **1a** molecules stacked face-to-face with the π–π distance found in the crystal structure of **1a**.

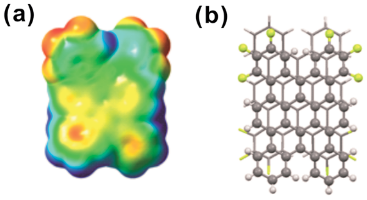

Fig. 7 (a) Molecular electrostatic potential of **1h** and (b) dimer of **1h** with the top molecule shown in a ball and stick model and arranged in the same orientation as that shown in (a) and the antiparallel bottom molecule shown in wireframe.

molecular dipole moments, but it does not show a shorter π⋯π distance than that of symmetrical **TFTBC** (Table 2). Secondly and more importantly, dichloro **1c** packs in a parallel arrangement between layers, which is not favorable in terms of the alignment of molecular dipole moments.

With larger substituents than **1a–1c**, methyl-substituted **1d**, trifluoromethyl-substituted **1e**, and *t*-butyl-substituted **1f** (Fig. 5d) do not pack in a parallel manner. Because the molecular planes of neighboring molecules in the π stacking direction are unparalleled to each other, it is not possible to obtain d_{l}, d_{s} and π⋯π distances for these compounds. For **1d** and **1f**, there are dimers in which the molecules rotating 90 degrees between layers in the crystal structures (*e.g.*, perpendicular dimers **2–3** in Fig. 5d), while for **1e** the rotation is 180 degrees and molecules shift along the long molecular axis. Along the π-stacking direction, molecules in any given dimer pair stack with a significant surface area overlapping with each other. Therefore, the crystal structure of all three compounds can still be categorized as 1-D packing. It is thus not surprising that needle-like crystals are found for **1d–1f**.

Some selected cell parameters are listed in Table 3. The theoretical results of reorganization energies (λ^+), electronic couplings (t^+) and charge transfer mobility (μ^+) for hole transport are shown in Table 2.

Because the substituents are attached to positions with small wave function coefficients in the HOMO, the effect of substituents on λ^+ is relatively small for **1a–h** (132 to 151 meV) in comparison to that for **TFTBC**, **TCTBC**, and 2,7,12,17-tetramethyl-TBC (**TMTBC**) (136 to 169 meV).[15] Small variations in λ^+ in a series of compounds could facilitate the structure–property correlation between crystal packing and mobility. For example, it is difficult to deduce the packing-mobility relationship between pentacene and perfluoropentacene because their reorganization energies differ by *ca.* 100 meV.[27] The large overlapping molecular surface along the π-stacking direction (*b* axis for **1a–c**, **1e**, and **1g**; *a* axis for **1f** and **1h**; *c* axis for **1d**) leads to 1-D packing and charge transporting. Therefore, we employ the unit length of the cell axis relevant to π-stacking to deduce the intermolecular distance (d_{axis}), which is then used in calculating the mobility of the charge carrier.[28] The largest mobility thus obtained is 0.91 cm^2 V^{-1} s^{-1} for hexafluoro derivative **1h**. As pointed out previously, the uniqueness of **1h** is that it has a large d_{l} (1.96 Å), but has the smallest shift d_{s} (0.24 Å). The other compounds that have relatively large

Table 3 Selected cell parameters of single crystals of **1**

	1a	1b	1c	1d	1e	1f	1g	1h
a (Å)	16.25	28.19	22.60	32.24	16.64	11.53	16.62	7.15
b (Å)	3.77	3.77	3.77	20.37	7.30	18.24	3.75	12.24
c (Å)	18.72	21.91	28.62	7.48	22.90	23.46	19.26	14.93
α (deg.)	90	90	90	90	90	87.11	90	74.98
β (deg.)	106.55	97.00	97.39	90	97.95	81.25	105.60	86.09
γ (deg.)	90	90	90	90	90	77.89	90	73.56
Space group	$P2_1/n$	$C2/c$	$P2_1/n$	$Pbca$	$P2_1/n$	$P\bar{1}$	$P2_1/n$	$P\bar{1}$

Published on 04 March 2014. Downloaded by Western Kentucky University on 29/10/2014 15:19:48.

predicted mobilities are **1a**, **1f**, and **1g**. Compounds **1a** and **1g** have very similar d_l and d_s values, whereas **1f** has a perpendicular dimer relationship in the crystal structures.[29]

SCFET device properties

Crystallites grown using the vapor phase transfer method were carefully examined under an optical microscope for their integrity and chosen for device fabrication. The single crystal field-effect transistors were prepared in the same fashion for all compounds, which exhibited typical p-type behavior. Five to nine samples for each compound were prepared and measured. The analyzed device characteristics are summarized in Table 4. The averaged values of hole-mobility of **1h**, **1f**, **1a**, and **1d** are noticeably larger than those of **1c**, **1e**, **1g**, and **1b**, and computational results gave plausible trends except for **1d** and **1g**. The exact source of discrepancy in the measured and calculated mobility is unclear. A worth-noting observation is that **1b** and **1g** exhibit the lowest mobility (both 0.06 cm^2 V^{-1} s^{-1}) among these compounds and both compounds are with an uncertainty of fluorine positions in the crystal structures. For compound **1a**, a negligible decrease of the averaged hole-mobility with a minimal deviation compared to our previous publication is obtained.[15] The typical output and transfer characteristics for compound **1d** are shown in Fig. 8.

As predicted by theoretical calculations, **1h** exhibits the highest value of hole-mobility among these compounds with mobility exceeding 1 cm^2 V^{-1} s^{-1}. Data in Table 2 show that the large mobility originates from the high electronic coupling value, which can in turn be rationalized by TBCs' HOMO distribution. The nodal planes of HOMOs of TBCs are mostly distributed along the short axis, but not the long axis (see Fig. 9 for HOMO of **1h**). As a result, shifting along the long axis can still result in high t^+. In Table 2, compounds with the largest t^+ values (49 meV for **1h** and 51 meV for **TCTBC**) have larger d_l than other compounds. Finally, it should be pointed out that TBCs with small substituents tend to pack with molecular planes parallel between layers, but TBCs with larger substituents (CH_3, CF_3, and *t*-butyl) tend to pack with their molecular planes unparallel to each other. Therefore, large substituents at the right positions could be the stepping stones to design high performance TBCs with 2-D packing.

Table 4 SCFET performance of tetrabenzocoronene derivatives

	Mobility (μ, cm^2 V^{-1} s^{-1})	Average mobility (μ_{avg})	On/off ratio	Threshold voltage (V_{th}, V)
1a	0.35–0.44	0.38 ± 0.030	10^4–10^5	(−26)–(−41)
1b	0.027–0.10	0.060 ± 0.025	10^3–10^5	(−17)–(−31)
1c	0.10–0.17	0.13 ± 0.027	10^2–10^4	(−7)–(−32)
1d	0.23–0.30	0.26 ± 0.026	10^3–10^5	(−7)–(−34)
1e	0.09–0.16	0.11 ± 0.0030	10^4–10^5	(−18)–(−38)
1f	0.35–0.64	0.45 ± 0.12	10^3–10^5	(−10)–(−18)
1g	0.044–0.090	0.061 ± 0.014	10^2–10^4	(−21)–(−28)
1h	0.842–1.19	1.06 ± 0.13	10^3–10^5	(−30)–(−35)

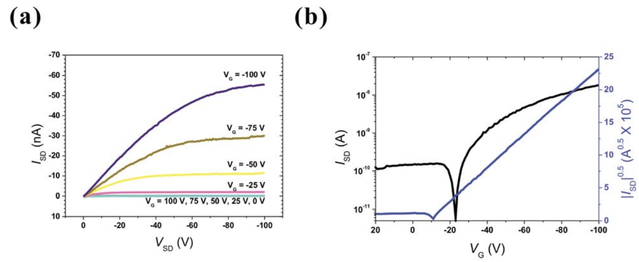

Fig. 8 (a) Output and (b) transfer characteristics of **1d**.

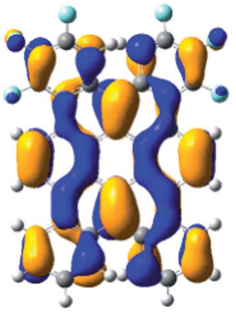

Fig. 9 The highest occupied molecular orbital of hexafluorinated **1h**.

Conclusion

In conclusion, a new series of non-planar and fused aromatic compounds, namely tetrabenzo[*a*,*d*,*j*,*m*]coronenes with unsymmetrical substitution were synthesized, characterized, and their single crystals were prepared for X-ray analyses as well as SCFET device fabrication. The strong dipole repulsion of the fluoro-containing derivatives leads to molecular packing in an anti-parallel manner, whereas the bulky alkyl substituents cause the molecules between layers to shift significantly in crystal packing. The subtle structural perturbation resulting from the substitution lead to variation in the transfer integral as well as reorganization energy and thus the mobility, as calculated using the hopping model. The calculated data seem to be in reasonable agreement with the experimental measurements. Among these, the SCFET with hexa-fluorinated **1h** as the channel material and parylene-N as the gate insulator gave a hole-mobility as high as 1.19 cm^2 V^{-1} s^{-1}. The result suggests that the perturbation caused by substituents in terms of shifts in the packing may have different effects on the transfer integral, depending on the distribution of the HOMO orbital.

Acknowledgements

The authors wish to thank the National Science Council, Taiwan and Academia Sinica for the financial support of the work. They also thank the National Center for High-Performance Computing and the Computing Center of Academia Sinica for providing computational resources.

Published on 04 March 2014. Downloaded by Western Kentucky University on 29/10/2014 15:19:48.

Notes and references

1 (*a*) G. Gelinck, P. Heremans, K. K. Nomoto and T. D. Anthopoulos, *Adv. Mater.*, 2010, **22**, 3778–3798; (*b*) M. Muccini, *Nat. Mater.*, 2006, **5**, 605–613; (*c*) C. D. Dimitrakopoulos and P. R. L. Malenfant, *Adv. Mater.*, 2002, **14**, 99–117; (*d*) H. Dong, C. Wang and W. Hu, *Chem. Commun.*, 2010, **46**, 5211–5222; (*e*) H. Klauk, *Chem. Soc. Rev.*, 2010, **39**, 2643–2666; (*f*) A. R. Murphy and J. M. J. Frchet, *Chem. Rev.*, 2007, **107**, 1066–1096; (*g*) M. E. Roberts, A. N. Sokolov and Z. Bao, *J. Mater. Chem.*, 2009, **19**, 3351–3363.

2 C. Wang, H. Dong, W. Hu, Y. Liu and D. Zhu, *Chem. Rev.*, 2012, **112**, 2208–2267.

3 C. A. Di, Y. Q. Liu, G. Yu and D. B. Zhu, *Acc. Chem. Res.*, 2009, **42**, 1573–1583.

4 (*a*) V. Podzorov, *MRS Bull.*, 2013, **38**, 15–24; (*b*) L. Jiang, H. Dong and W. Hu, *J. Mater. Chem.*, 2010, **20**, 4994–5007; (*c*) C. Reese and Z. N. Bao, *J. Mater. Chem.*, 2006, **16**, 329–333; (*d*) R. W. I. de Boer, M. E. Gershenson, A. F. Morpurgo and V. Podzorov, *Phys. Status Solidi*, 2004, **201**, 1302–1331; (*e*) M. E. Gershenson, V. Podzorov and A. F. Morpurgo, *Rev. Mod. Phys.*, 2006, **78**, 973–989; (*f*) J. Takeya, C. Goldmann, S. Haas, K. P. Pernstich, B. Ketterer and B. Batlogg, *J. Appl. Phys.*, 2003, **94**, 5800–5804; (*g*) R. W. I. de Boer, T. M. Klapwijk and A. F. Morpurgo, *Appl. Phys. Lett.*, 2003, **83**, 4345–4347.

5 (*a*) D. Boudinet, M. Benwadih, S. Altazin, J.-M. Verilhac, E. De Vito, C. Serbutoviez, G. Horowitz and A. Facchetti, *J. Am. Chem. Soc.*, 2011, **133**, 9968–9971; (*b*) M. M. Islam, S. Pola and Y.-T. Tao, *ACS Appl. Mater. Interfaces*, 2011, **3**, 2136–2141.

6 (*a*) V. C. Sundar, J. Zaumseil, V. Podzorov, E. Menard, R. L. Willett, T. Someya, M. E. Gershenson and J. A. Rogers, *Science*, 2004, **303**, 1644–1646; (*b*) J. Takeya, M. Yamagishi, Y. Tominari, R. Hirahara, Y. Nakazawa, T. Nishikawa, T. Kawase, T. Shimoda and S. Ogawa, *Appl. Phys. Lett.*, 2007, **90**, 102120.

7 (*a*) A. S. Molinari, H. Alves, Z. Chen, A. Facchetti and A. F. Morpurgo, *J. Am. Chem. Soc.*, 2009, **131**, 2462–2463; (*b*) N. A. Minder, S. Ono, Z. Chen, A. Facchetti and A. F. Morpurgo, *Adv. Mater.*, 2012, **24**, 503–508; (*c*) M. M. Islam, S. Pola and Y.-T. Tao, *Chem. Commun.*, 2011, **47**, 6356–6358.

8 V. Coropceanu, J. Cornil, D. A. da Silva, Y. Olivier, R. Silbey and J. L. Bredas, *Chem. Rev.*, 2007, **107**, 926–952.

9 O. Kwon, V. Coropceanu, N. E. Gruhn, J. C. Durivage, J. G. Laquindanum, H. E. Katz, J. Cornil and J. L. Bredas, *J. Chem. Phys.*, 2004, **120**, 8186–8194.

10 E. V. Anslyn and D. A. Dougherty, *Modern Physical Organic Chemistry*, University Science Book, Sausalito, CA, 2006.

11 (*a*) H. Moon, R. Zeis, E. J. Borkent, C. Besnard, A. J. Lovinger, T. Siegrist, C. Kloc and Z. N. Bao, *J. Am. Chem. Soc.*, 2004, **126**, 15322–15323; (*b*) J. E. Anthony, J. S. Brooks, D. L. Eaton and S. R. Parkin, *J. Am. Chem. Soc.*, 2001, **123**, 9482–9483; (*c*) J. E. Anthony, D. L. Eaton and S. R. Parkin, *Org. Lett.*, 2002, **4**, 15–18.

12 S. Xiao, M. Myers, Q. Miao, S. Sanaur, K. Pang, M. L. Steigerwald and C. Nuckolls, *Angew. Chem., Int. Ed.*, 2005, **44**, 7390–7394.

13 (*a*) M. M. Islam, F. Valiyev, H. Lu, M. Kuo, I. Chao and Y.-T. Tao, *Chem. Commun.*, 2011, **47**, 2008–2010; (*b*) I. Oonishi, S. Fujisawa, J. Aoki, Y. Ohashi and Y. Sasada, *Bull. Chem. Soc. Jpn.*, 1986, **59**, 2233–2238; (*c*) S. Fujisawa, I. Oonishi, J. Aoki, Y. Ohashi and Y. Sasada, *Bull. Chem. Soc. Jpn.*, 1982, **55**, 3424–3428.

14 X. Zhang, X. Jiang, K. Zhang, L. Mao, J. Luo, C. Chi, H. S. O. Chan and J. Wu, *J. Org. Chem.*, 2010, **75**, 8069–8077.

15 S. Pola, C.-H. Kuo, W.-T. Peng, M. M. Islam, I. Chao and Y. T. Tao, *Chem. Mater.*, 2012, **24**, 2566–2571.

16 V. Podzorov, V. M. Pudalov and M. E. Gershenson, *Appl. Phys. Lett.*, 2003, **82**, 1739–1741.

17 S. M. Sze, *Semiconductor Device Physics and Technology*, Wiley, New York, 2nd edn, 2001, ch. 6, p. 169.

18 M.-Y. Kuo, H.-Y. Chen and I. Chao, *Chem.–Eur. J.*, 2007, **13**, 4750–4758.

19 M. J. Frisch, G. W. Trucks, H. B. Schlegel, G. E. Scuseria, M. A. Robb, J. R. Cheeseman, G. Scalmani, V. Barone, B. Mennucci, G. A. Petersson, H. Nakatsuji, M. Caricato, X. Li, H. P. Hratchian, A. F. Izmaylov, J. Bloino, G. Zheng, J. L. Sonnenberg, M. Hada, M. Ehara, K. Toyota, R. Fukuda, J. Hasegawa, M. Ishida, T. Nakajima, Y. Honda, O. Kitao, H. Nakai, T. Vreven, J. A. Montgomery Jr, J. E. Peralta, F. Ogliaro, M. Bearpark, J. J. Heyd, E. Brothers, K. N. Kudin, V. N. Staroverov, R. Kobayashi, J. Normand, K. Raghavachari, A. Rendell, J. C. Burant, S. S. Iyengar, J. Tomasi, M. Cossi, N. Rega, N. J. Millam, M. Klene, J. E. Knox, J. B. Cross, V. Bakken, C. Adamo, J. Jaramillo, R. Gomperts, R. E. Stratmann, O. Yazyev, A. J. Austin, R. Cammi, C. Pomelli, J. W. Ochterski, R. L. Martin, K. Morokuma, V. G. Zakrzewski, G. A. Voth, P. Salvador, J. J. Dannenberg, S. Dapprich, A. D. Daniels, Ö. Farkas, J. B. Foresman, J. V. Ortiz, J. Cioslowski, and D. J. Fox, *Gaussian 09, A.1 Revision*, Gaussian Inc., Wallingford CT, 2009.

20 For calculation details and performance of this theory level on internal reorganization energy, see (*a*) N. E. Gruhn, D. A. da Silva Filho, T. G. Bill, M. Malagoli, V. Coropceanu, A. Kahn and J. L. Brédas, *J. Am. Chem. Soc.*, 2002, **124**, 7918–7919; (*b*) M. Malagoli, V. Coropceanu, D. A. da Silva and J. L. Bredas, *J. Chem. Phys.*, 2004, **120**, 7490–7496; (*c*) Y.-C. Chang and I. Chao, *J. Phys. Chem. Lett.*, 2010, **1**, 116–121.

21 G. te Velde, F. M. Bickelhaupt, E. J. Baerends, C. Fonseca Guerra, S. J. A. van Gisbergen, J. G. Snijders and T. Ziegler, *J. Comput. Chem.*, 2001, **22**, 931–967.

22 (*a*) K. Senthilkumar, F. C. Grozema, F. M. Bickelhaupt and L. D. A. Siebbeles, *J. Chem. Phys.*, 2003, **119**, 9809–9817; (*b*) P. Prins, K. Senthilkumar, F. C. Grozema, P. Jonkheijm, A. P. H. J. Schenning, E. W. Meijer and L. D. A. Siebbeles, *J. Phys. Chem. B*, 2005, **109**, 18267–18274.

This journal is © The Royal Society of Chemistry 2014

Published on 04 March 2014. Downloaded by Western Kentucky University on 29/10/2014 15:19:48.

23 (*a*) A. N. Sokolov, S. Atahan-Evrenk, R. Mondal, H. B. Akkerman, R. S. Sánchez-Carrera, S. Granados-Focil, J. Schrier, S. C. B. Mannsfeld, A. P. Zoombelt, Z. Bao and A. Aspuru-Guzik, *Nat. Commun.*, 2011, **2**, 437; (*b*) V. Stehr, J. Pfister, R. F. Fink, B. Engels and C. Deibel, *Phys. Rev. B: Condens. Matter Mater. Phys.*, 2011, **83**, 155208; (*c*) Y. Song, C. Di, X. Yang, S. Li, W. Xu, Y. Liu, L. Yang, Z. Shuai, D. Zhang and D. Zhu, *J. Am. Chem. Soc.*, 2006, **128**, 15940–15941; (*d*) W. Q. Deng and W. A. Goddard III, *J. Phys. Chem. B*, 2004, **108**, 8614–8621; (*e*) H. Li, J.-L. Bredas and C. Lennartz, *J. Chem. Phys.*, 2007, **126**, 164704; (*f*) S. E. Koh, C. Risko, D. A. da Silva, O. Kwon, A. Facchetti, J.-L. Brédas, T. J. Marks and M. A. Ratner, *Adv. Funct. Mater.*, 2008, **18**, 332–340.

24 P. M. Donovan and L. T. Scott, *J. Am. Chem. Soc.*, 2004, **126**, 3108–3112.

25 N. Miyaura and A. Suzuki, *Chem. Rev.*, 1995, **95**, 2457–2483.

26 (*a*) T. S. Navale, K. Thakur and R. Rathore, *Org. Lett.*, 2011, **13**, 1634–1637; (*b*) K. N. Plunkett, K. Godula, C. Nuckolls, N. Tremblay, A. C. Whalley and S. Xiao, *Org. Lett.*, 2009, **11**, 2225–2228.

27 H. Y. Chen and I. Chao, *Chem. Phys. Lett.*, 2005, **401**, 539–545.

28 In our previous study on TBCs, $d_{\mathrm{c-c}}$ was used to calculate to the mobility. The only compound affected by replacing $d_{\mathrm{c-c}}$ with d_{axis} is **TMTBC**, whose mobility changed from 0.18 to 0.13 $\mathrm{cm^2\ V^{-1}\ s^{-1}}$ as shown in Table 2.

29 Along the π-stacking direction of the crystal structure, all dimers are perpendicular to **1d** and there is only one t^+ value for dimeric electronic coupling. For **1f**, the dimeric relationship along the π-stacking direction is more complicated as shown in Fig. 5d. The t^+ values for dimer$_{1-2}$, dimer$_{2-3}$, and dimer$_{3-1'}$ are 56, 40, and 79 meV, respectively.